Cellular Potts Model on Collective Cell Movement

Tsuyoshi HIRASHIMA

Graduate School of Medicine, Kyoto University

1   Preface

Collective cell movement is an essential process in many events of all animals, including wound healing and embryonic development although our understanding for what attributes the emergence of collective cell movement is far from complete. Modeling multicellular behavior leads to further understanding of collective cell movement. In this report, I first introduce the Cellular Potts Model, a cell-oriented model that can express the multicellular behavior. Next, I show that the model results obtained by numerical simulations with quantified data well matches the experimental observations of multicellular movement. Finally, I report that the model including dynamics of direction of each individual cell applied in this study can represent characteristic multicellular behavior observed in experiments.

2   Cellular Potts Model

In this section, I explain about the Cellular Potts Model (CPM). The CPM represents morphology of each cell as a connection of lattices sites; therefore, an assembly of different indexed clusters of lattice site whose index has the same value represents a group of cells (Fig.1A). In the model, a state transition resulting from lattice replacement between neighboring ones is preferred for decreasing the energy of the system H [1]. The energy adopted in the model contains the minimal factors necessary to capture the multicellular dynamics, such as interfacial energy, cell volume constraint, cell division, and cell migration (Fig. 1B). H is defined as

$$H = \sum_{\vec{x},\vec{x}'} J_{\tau(\sigma_{\vec{x}})\tau(\sigma_{\vec{x}'})}\left(1-\delta_{\sigma_{\vec{x}}\sigma_{\vec{x}'}}\right)+\lambda_v\sum_{\sigma}\left(V_\sigma - V_0\right)^2 ,\tag{1}$$

where $\vec{x}$ and $\vec{x}'$ each represent a position of lattice site, σ is an index labeled on a specified lattice, τ represents an attribute i.e., cell or medium, J is the interfacial energy between cell-cell or cell-medium, λ_v is the magnitude of cell volume constraint, V_σ is the current cell volume, V_0 is the ideal cell volume, and δ represents the Kronecker delta. The interfacial energy per unit length J determines the adhesion strength of the interacting

materials, such as cell-cell or cell-medium, and λ_v represents resistance to cell compression/expansion.

The system transition occurs stochastically by a lattice-based Monte Carlo method; that is, the labeled value of a randomly chosen lattice site $\sigma_{\vec{x}}$ is attempted to be replaced by a different labeled value of its neighboring lattice site randomly chosen $\sigma_{\vec{x}'}$. The transition is realized by evaluating the change in energy ΔH associated with its replacement. Even if ΔH is positive, the replacement occurs at a given probability. The change in energy resulting from the state transition ΔH contains one for the cell migration:

$$\Delta H = H_{after} - H_{before} - E_m, \tag{2}$$

where the migration energy E_m defined as

$$E_m = \lambda_m \sum_\sigma \tilde{a}_\sigma \cdot \tilde{v}_\sigma . \tag{3}$$

$\vec{a}$ represents the vector of the front-rear axis of cell migration, $\vec{v}$ represents the vector connecting from the position of cell to a candidate position of the cell shifted by the replacement, and λ_m is the intensity of cell migration. The tilde over each letter indicates the unit vector (Fig. 1C).

To update the front-rear axis accompanied by the state transition, we propose the following:
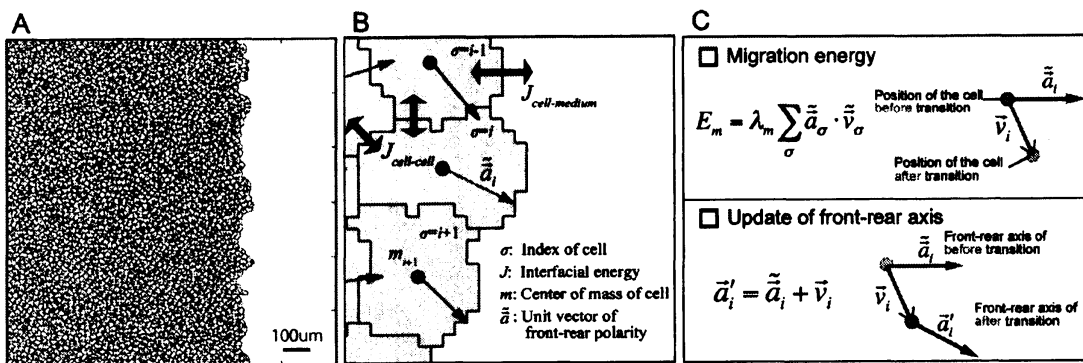

Figure 1 Cellular Potts Model. (A) An example of model simulation. (B) Schematic explanation of energies used in the model. (C) Migration energy and update rule of front-rear axis.

$$\vec{a}_i' = \tilde{\vec{a}}_i + \vec{v}_i \qquad (4)$$

where $\vec{a}'$ is the updated front-rear axis, and the suffix i represents the cells that change position by the lattice replacement.

To realize the minimum system energy at equilibrium, the state transition occurs stochastically with biological noise such as cytoskeletal fluctuations in the following:

$$\Pr\begin{bmatrix} \text{transition} \\ \text{is realized} \end{bmatrix} = \begin{cases} \exp[-\beta\Delta H], & \text{if } \Delta H > 0 \\ 1, & \text{if } \Delta H \leq 0 \end{cases} \qquad (5)$$

β represents the magnitude of the biological such as membrane fluctuations. See [1, 2] for more details. [3] is a good primer for ones who want to make a CPM program.

3   Experiments

In this section, I show experimental results about dependence of multicellular movement and that of intercellular adhesion on Ca^{2+} concentrations included in culture medium. The concentrations of Ca^{2+} I used were 0.075, 0.15, 0.75, and 1.5 mM.

For the measurement of multicellular movement, I used a conventional free-injury experimental system, in which removing a non-toxic plastic sheet allowed confluent cultured cells to move to a free space. To quantify the dynamics of individual cells, we conducted particle image velocimetry (PIV) analysis for the time-lapse images of cell movement captured every 10 minutes. Using the results of the PIV analysis, we computed the average velocity of particles within a small fixed grid between two temporal sequential images.

For the measurement of intercellular adhesion, I adopted a femtosecond-laser-based assay. See [4] for the details of measurement procedures. From this analysis, I found that the relative intercellular adhesion strength for each Ca^{2+} treatment W, i.e., W^X for X=0.075, 0.15, 0.75, and 1.5, was quantified; $W^{0.075}=1.0$, $W^{0.15}=1.6$, $W^{0.75}=6.0$, and $W^{1.5}=13.2$.

4   Quantities for Collective Cell Movement

To measure the directional and cohesive cell movement, three quantities were introduced: (I) moving distance of front edge, (II) degree of forward movement, and (III) spatial correlation length. The more directional/cohesive the movement becomes, the greater the degree of forward movement/spatial correlation length.

The degree of forward movement is defined as follows:

$$\left\langle \sum_i^N \tilde{u}_i^x / N \right\rangle,$$

(6)

where i is the index of cells, $\tilde{u}_i^x$ is the x component of the unit vector of cell displacement per 10 minutes, and N is the total number of cells in the observation window. A tilde and $\langle \cdot \rangle$ indicate the unit vector and time average, respectively.

For the spatial correlation length, I first calculated the spatial correlation function ϕ:

$$\phi(R) = \frac{\sum_{i=1}^N \Delta \vec{u}_i \cdot \Delta \vec{u}_{i+k}}{\sqrt{\sum_{i=1}^N \Delta \vec{u}_i^2} \sqrt{\sum_{i=1}^N \Delta \vec{u}_{i+k}^2}},$$

(7)

where $\Delta \vec{u}_i$ is a deviation from its spatial mean $\sum_{i=1}^N \vec{u}_i$. The spatial index k was converted to the distance in radial directions R. Then, the spatial correlation length is defined as follows:

$$\left\langle \frac{1}{2} \int_0^{R_{Max}} \phi dR \right\rangle.$$

(8)

5 Parameters

I set one pixel of the simulation space as 2 μm, and the computer simulation was performed in 600×600 pixel^2. The ideal cell volume was determined by some images, $V_0 = 100$. As an initial distribution of the front-rear axis, we assumed that the direction of front-rear axis had a uniform distribution, and that cell volume was slightly compressed, $V_0 = 95$. The initial variation of V_0 did not affect conclusions qualitatively.

As mentioned in previous studies [1,5], the energy to maintain intercellular adhesion was defined as $\gamma = J_{cell-medium} - J_{cell-cell}/2$, where $J_{cell-cell}$ and $J_{cell-medium}$ are each the interfacial energy between the cells and that between the cell and medium. In this study, the laser-used estimation revealed the relative strength of intercellular adhesion W among Ca^{2+} treatments, i.e., $W^X = \gamma^X / \gamma^{0.075}$ for $X = 0.075$, 0.15, 0.75, and 1.5. I assumed that the interfacial energy between cell and medium is proportional to that between cells. I set

$J_{cell-medium} = 1.5 \ J_{cell-cell}$, leading to $\gamma^X = J^X_{cell-cell}$; the qualitative results did not change significantly when the constant value changed. For numerical simulations the parameter values were given as: γ=0.1-10.0, λ_v=0.1-10.0, λ_m=1.0-10.0, and β=1-2. In the model, a cell divides with a constant probability μ at each Monte Carlo step, and the cell division probability was given as μ=10^{-4} from measured data (not shown).

6 Comparison between Experimental Data and Model Results

Over the parameter range I did extensive numerical simulations and compared results generated by the simulations with experimental results. The PIV analysis for the experimental observation revealed that the front edge in the group of cells moved farther for higher Ca^{2+} concentrations (Jonckheere-Terpstra test, $P \ll 0.001$ for each time, n=3 for each treatment), and more directional and cohesive movement was generated for the higher Ca^{2+} treatments (Jonckheere-Terpstra test, $P \ll 0.001$, n=4 for each treatment) (Fig. 2).

In consideration of the experimental results, I examined the dependence of three quantities for multicellular movement on the relative strength of intercellular adhesion corresponding to each Ca^{2+} treatments. I found that the model results well matched the trend of experimental observation (n=2000 for each value of relative adhesion strength, Fig. 2). Indeed, the movement distance of the front edge became long, and the two order quantities for the collectivity of multicellular movement also increased in response to the increase of intercellular adhesion strength.
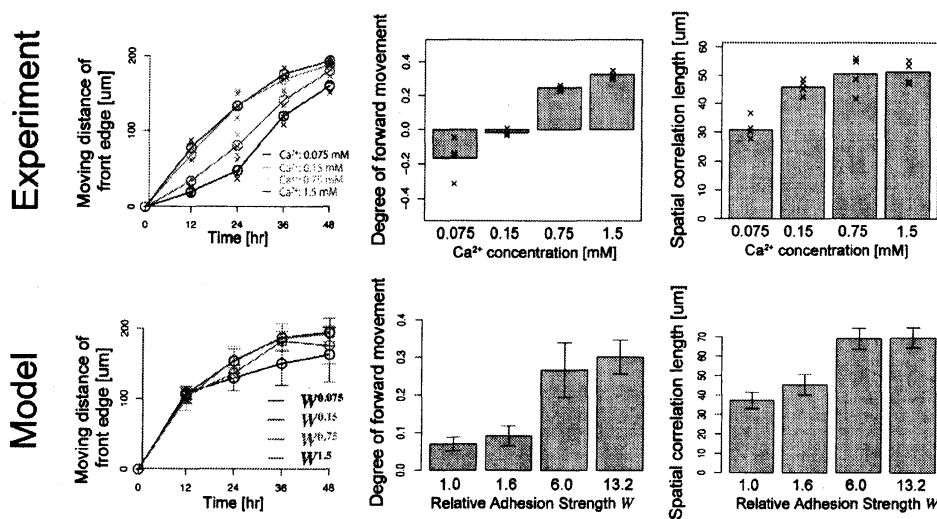

Figure 2 Comparison between experimental and model results. The dependence of three quantities on the Ca^{2+} treatments (upper) and that on the corresponding relative adhesion strength (below) are shown.

In conclusion, the experiments and the numerical simulation of model revealed that the strength of intercellular adhesion is a sufficient factor for the emergence of collective cell movement.

7 A Key Factor for Modeling Multicellular Movement: Cell Polarity

In the last section, I show that the dynamics of cell polarity for the cell migration given to individual cells is a key point to express multicellular behavior in mathematical modeling. I observed multicellular movement of a relatively small number of cells, i.e., 2, 3, and 8 cells so as to capture the movement as simple as possible. Interestingly, I found that a small number of cells moved cooperatively maintaining their neighboring connections, and exhibited a swirling movement in all cases. The figure 3 shows only the case of 3-cells movement. Note that tracking data of a single cell in the 3-cells movement clearly shows a circling motion.

The numerical simulation of the model for a small number of cells was performed to test whether the model can represent the characteristic swirling motion. Surprisingly, the model including Eq. (4) well represented the characteristic swirling behavior in all situations: 2-cells, 3-cells, and 8-cells. Also, I confirmed that the multicellular swirling behavior was realized in most of the parameter range used in this study.
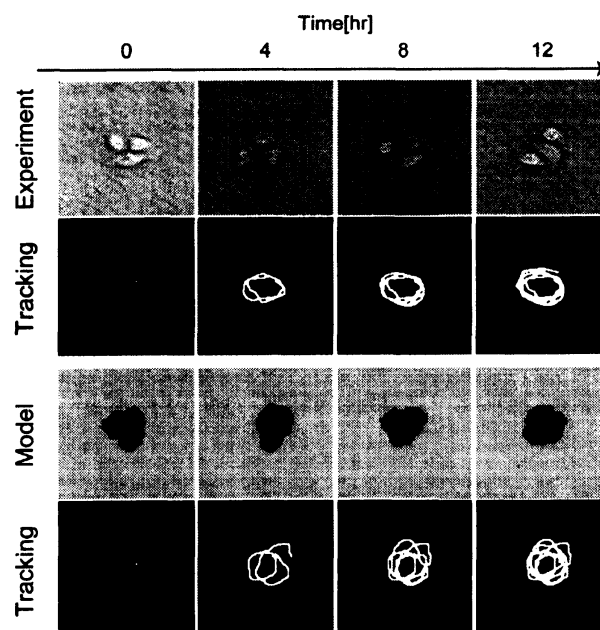

Figure 3 3-cells movement and tracking of a single cell. Tracking lines were depicted using the ImageJ. The characteristic swirling behavior is seen in the experiment and in the model simulation.

We determined Eq. (4) according to an earlier study [6], in which a basic idea of temporal update of cell polarity vector that can model multicellular sprout formation is proposed. We suggest the dynamics of front-rear axis as Eq. (4) in a heuristic manner this time. For further development data collection of multicellular behaviors in various situations and statistical modeling using the data are necessary to build a better mathematical model of multicellular behavior.

8 References

[1] Glazier, J. A. and Graner, F. (1993). Simulation of the Differential Adhesion Driven Rearrangement of Biological Cells. *Physical Review E* 47, 2128-2154.

[2] Hirashima, T., Iwasa, Y. and Morishita, Y. (2009). Dynamic modeling of branching morphogenesis of ureteric bud in early kidney development. *Journal of Theoretical Biology* 259, 58-66.

[3] Jiang, Y. (1998). Cellular Pattern Formation. Ph.D. Dissertation for University of Notre Dame, Department of Physics.

[4] Hosokawa, Y., Hagiyama, M., Iino, T., Murakami, Y. and Ito, A. (2011). Noncontact estimation of intercellular breaking force using a femtosecond laser impulse quantified by atomic force microscopy. *Proceedings of the National Academy of Sciences of the United States of America* 108, 1777-1782.

[5] Davies, J.T. and Rideal, E.K. (1963). *Interfacial Phenomena*. 2nd ed., New York: Academic Press Inc.

[6] Szabo, A. and Czirok, A. (2010). The Role of Cell-Cell Adhesion in the Formation of Multicellular Sprouts. *Mathematical Modelling of Natural Phenomena* 5, 106-122.

Acknowledgement

Graduate School of Medicine, Kyoto University

Kyoto 606-8501, JAPAN

E-mail address: tsuyoshi.hirashima@gmail.com

京都大学・医学研究科　平島　剛志